Ballistic behavior and trapping of self-driven particles in a Poiseuille flow

Leonardo Apaza
Faculty of Pure and Natural Sciences, Universidad Mayor de San Andres, La Paz, Bolivia

Mario Sandoval*
Department of Physics, Universidad Autonoma Metropolitana-Iztapalapa, Distrito Federal 09340, Mexico
(Received 14 February 2016; revised manuscript received 24 May 2016; published 9 June 2016)

We study the two- and three-dimensional dynamics of a Brownian self-driven particle at low Reynolds number in a Poiseuille flow. A deterministic analysis is also performed and we find that under certain conditions the swimmer becomes trapped, thus performing closed orbits as observed in related experiments. Further analysis enables us to provide an analytic expression to achieve this trapping phenomenon. We then turn to Brownian dynamics simulations, where we show the effect of a Poiseuille flow, self-propulsion, and confinement on the diffusion of the swimmer in both two and three dimensions. It is found that for long times the mean-square displacement (MSD) along the flow direction is always quadratic in time, whereas for shorter times (before the particle reaches the walls) its MSD has also a quartic time behavior. It is also found that self-propelled particles will spread less in a Poiseuille flow than passive ones under the same circumstances.

DOI: 10.1103/PhysRevE.93.062602

I. INTRODUCTION

The study of micrometric and nanometric self-propelled (active) particles has recently received much attention [1–8]. Many phenomena in nature involving the motion of micro-organisms that self-propel have proved to be very relevant [9–13]. Further, scientists have found self-propelled particles useful elements of study in the field of active matter [14]. In addition, bioengineers are already mimicking propulsion strategies of natural swimmers (micro-organisms) and building self-propelled micromachines [15–18]. These microrobots may be in charge of carrying specialized drugs to particular regions inside our body, as well as detecting and diagnosing diseases [19–21]. The latter applications are very relevant in medicine since less intrusive treatment options may be very close to becoming a reality.

Because some microrobots and micro-organisms are small enough to be affected by thermal fluctuations, their motion will follow random paths (Brownian motion) [3,22]. Moreover, the net displacement of those Brownian microswimmers may also be affected by external flows, like marine bacteria affected by oceanic turbulence or natural and synthetic swimmers inside the human body being subject to flowing bodily fluids [23,24]. Previous works have already studied the effect of moving fluids on the diffusion of passive (not self-propelled) Brownian spherical particles. For example, Foister and van de Ven [25] found that a Brownian passive spherical particle, under the effect of a shear flow, has a mean-square displacement (MSD) along the flow direction proportional to the third power of time. They even found that in the presence of an external extensional flow, the MSD of the Brownian passive particle behaves exponentially in time. Other nonlinear external velocity fields such as the classical Poiseuille flow were also considered by Foister and van de Ven [25].

The consequences of moving fluids on self-propelled particles have also been analyzed. Jones *et al.* [26] calculated, for non-Brownian particles, the direction of swimming of bottom-heavy micro-organisms immersed in shear flows. Bearon and Pedley [27] worked with chemotactic bacteria and found an advection-diffusion equation for the cell density under the effect of a shear flow. More recently, ten Hagen *et al.* [28] found, in a two-dimensional (2D) domain, the MSD tensor of a spherical Brownian self-propelled particle in a shear flow. They obtained that the MSD along the flow direction behaves like $\sim t^3$. A generalization of their work to the case of a swimmer immersed in a general linear flow, in both two and three dimensions, was made by Sandoval *et al.* [29,30]. Recently, Zöttl and Stark [31,32] performed theoretical studies and elucidated the dynamics of a deterministic spherical and elongated swimmer under a Poiseuille flow in two and three dimensions. They concluded that the swimmer may perform swinging and tumbling orbits. In addition, Costanzo *et al.* [33] and Chilukuri *et al.* [34] computationally found the effect of a Poiseuille flow on the transversal concentration of Brownian swimmers inside a pipe. They found aggregation and upstream swimming. An experimental confirmation of the works from Zöttl [31,32], Costanzo *et al.* [33], and Chilukuri *et al.* [34] was made by Rusconi *et al.* [35], who built a microfluidic devise where a Poiseuille flow was imposed.

From the latter references, one can see that there is a significative effort in understanding the behavior of self-propelled micrometric particles under external flows. In this paper we analyze the effect of a Poiseuille flow on the diffusion of a Brownian self-propelled particle (swimmer) confined in a channel (two dimensions) and a cylinder (three dimensions) and elucidate the temporal scaling of its MSD along the flow direction. The swimming particle is considered to be spherical given that around 21% of living bacteria possess this form [36] and that some artificial swimmers such as self-catalytic colloidal spheres [5,8,37,38] and active droplets [39,40] also have this geometry. We model the activity of the particle with an assumed constant swimming velocity in its body frame and consider that rotational and translational Brownian motion affects our swimmer. Other rotational mechanisms such as run and reverse [12] or run and tumble [3,41] are not taken into

*sem@xanum.uam.mx

account. We start by setting up the problem in Sec. II and study the deterministic dynamics of the swimmer in Sec. III. Here we observe that the swimmer may follow closed paths; in other words, the swimmer may become trapped. We thus provide an analytical condition to observe this trapping phenomenon. In Secs. IV and V we use Brownian dynamics simulations to calculate the MSD of an active particle in a channel or cylinder subject to a Poiseuille flow. A comparison among two- and three-dimensional simulations is also performed. It is concluded that the effect of a Poiseuille flow in a channel or cylinder is to generate a long-term quadratic time dependence of the MSD along the flow direction. From a frame moving with a velocity equal to v_m (with respect to the laboratory frame), one can also observe a quartic time dependence of the MSD along the flow direction for active particles. It is found that the activity of the particle may screen this quartic dependence even in the moving frame. We also report that trapping is observed in three dimensions. Finally, we use a dipole approximation model to incorporate wall hydrodynamic effects (HEs). This model suggests that HEs do not seem to affect the swimmer's diffusion.

II. MODEL

We consider a spherical self-propelled particle (swimmer) of radius a inside a channel of cross section $2R$, swimming in a two-dimensional fluctuating environment at temperature T. This particle is also subject to a Poiseuille flow of the form $\mathbf{U}_\infty = v_m[1 - x_2^2/R^2]\mathbf{i}$ (see Fig. 1). Here v_m is the fluid's velocity along the center of the channel. The swimmer is free to rotate along the azimuthal direction θ and its dynamics is described by its translational velocity $\dot{\mathbf{x}}(t)$ and angular velocity $\mathbf{\Omega}(t)$. Here $\mathbf{x}(t) = [x_1(t), x_2(t)]$ represents the swimmer's position, while the overdot stands for a time derivative. In this model the walls are assumed to be specular and do not affect the swimmer's rotation. In Sec. VI we include a model where hydrodynamic interactions among the swimmer and walls are taken into account. Note that in the rest of the paper the set $\{\mathbf{i},\mathbf{j},\mathbf{k}\}$ represent unit vectors. Thermal forces in translation $\mathbf{f}$ and rotation $\mathbf{g}$ are modeled as zero-mean random variables whose correlations, according to the fluctuation-dissipation theorem, are given by $\langle f_i(t) f_j(t')\rangle = 2k_B T R_U \delta_{ij}\delta(t-t')$ and $\langle g_i(t) g_j(t')\rangle = 2k_B T R_\Omega \delta_{ij}\delta(t-t')$, respectively, where $\langle\cdot\rangle$ represents ensemble averaging [42].

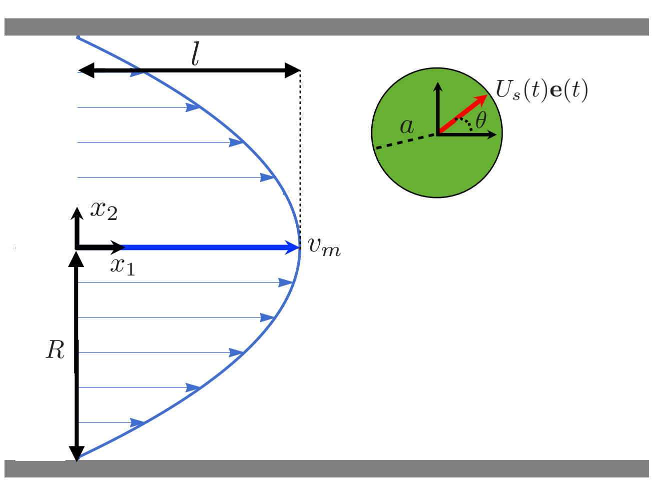

FIG. 1. Schematics of the studied problem.

At low Reynolds number, the balance of forces and torques on the particle leads to

$$\mathbf{R}_U(\dot{\mathbf{x}} - \mathbf{U}_s - \mathbf{U}_\infty) = \mathbf{f}, \quad \mathbf{R}_\Omega(\mathbf{\Omega} - \mathbf{\Omega}_\infty) = \mathbf{g}, \tag{1}$$

where $\mathbf{\Omega}_\infty$ is the angular velocity of the particle induced by the Poiseuille flow, $\mathbf{U}_s = U_s(t)\mathbf{e}(t)$ is the swimming velocity along the director vector, $\mathbf{e}(t) = [\cos\theta(t), \sin\theta(t)]$ (with the origin at the center of the particle), and $U_s(t)$ is the instantaneous magnitude of the swimming velocity. In the rest of the paper and for simplicity, we assume a constant swimming velocity $U_s(t) = U=$ const. In Eq. (1), $\mathbf{R}_U = R_U\mathbf{I}$ and $\mathbf{R}_\Omega = R_\Omega\mathbf{I}$ are the viscous resistance coefficients ($R_U = 6\pi\eta a$ and $R_\Omega = 8\pi\eta a^3$ in a Newtonian fluid of viscosity η) and $\mathbf{I}$ is the unit tensor. Similarly, the director vector $\mathbf{e}$ follows the dynamics [43]

$$\dot{\mathbf{e}}(t) = \mathbf{\Omega}(t) \times e(t). \tag{2}$$

Thus, from Eq. (1), in combination with Eq. (2), together with the dimensionless variables $\tilde{x}_1 = x_1/l$ (here l is a characteristic length of the Poiseuille profile; see Fig. 1), $\tilde{x}_2 = x_2/l$, $\tilde{t} = (v_m/l)t$, $\varepsilon = l/R$, $u_d = U/v_m$, $\tilde{\mathbf{f}} = \mathbf{f}/R_U v_m$, and $\tilde{\mathbf{g}} = (l/R_\Omega v_m)\mathbf{g}$, we get the dynamics of the microswimmer

$$\dot{\tilde{x}}_1(\tilde{t}) = 1 - \varepsilon^2\tilde{x}_2^2(\tilde{t}) + u_d\cos\theta(\tilde{t}) + \tilde{f}_1(\tilde{t}), \tag{3}$$

$$\dot{\tilde{x}}_2(\tilde{t}) = u_d\sin\theta(\tilde{t}) + \tilde{f}_2(\tilde{t}), \tag{4}$$

$$\dot{\theta}(\tilde{t}) = \varepsilon^2\tilde{x}_2(\tilde{t}) + \tilde{g}(\tilde{t}). \tag{5}$$

Note that one degree of rotation has already been observed in experiments with spherical platinum-silica Janus particles in a solution of water and H_2O_2 [44]. Moreover, it is often the case that a two-dimensional model gives qualitative results similar to those of a fully three-dimensional problem [30]. This observation will be corroborated in Sec. V, where the present model is extended to three dimensions.

III. TRAPPING

In addition to Zöttl and Stark's contribution [31], we have found that under certain circumstances, a spherical swimmer in a Poiseuille flow may become trapped, that is, it may perform closed paths (see Fig. 3) due to an interplay between self-propulsion and the imposed external flow. A similar trapping phenomenon has been experimentally reported for a self-propelled ellipsoidal particle in a Poiseuille flow [35] but no further analytical analysis was performed. In order to find analytical conditions where trapping occurs, we use Eqs. (3)–(5) and neglect the stochastic forces, namely,

$$\dot{\tilde{x}}_1 = 1 - \varepsilon^2\tilde{x}_2^2 + u_d\cos(\theta), \tag{6}$$

$$\dot{\tilde{x}}_2 = u_d\sin(\theta), \tag{7}$$

$$\dot{\theta} = \varepsilon^2\tilde{x}_2. \tag{8}$$

In general, Eqs. (6)–(8) admit an analytical solution by using the Jacobi elliptic functions. However, with that general solution, one cannot determine the necessary condition to observe trapping. By analyzing the latter system under small oscillations, using the fact that trapping has been computationally observed for $u_d < 0$ (although trapping for $u_d > 0$ is also possible), and combining Eqs. (7) and (8), one gets

$$\theta(\tilde{t}) = \theta_0 \cos(\sqrt{|u_d|}\varepsilon\tilde{t}), \tag{9}$$

where the initial conditions $\tilde{x}_2(0) = 0$ and $\theta(0) = \theta_0$ were employed. Additionally, by dividing Eqs. (7) and (8) and integrating that result, one gets

$$\tilde{x}_2(\theta)^2 = -2\frac{|u_d|}{\varepsilon^2}[\cos(\theta_0) - \cos(\theta)]. \tag{10}$$

This equation is then substituted into Eq. (6), which gives

$$\dot{\tilde{x}}_1 = 1 + 2|u_d|\cos(\theta_0) - 3|u_d|\cos[\theta_0\cos(\sqrt{|u_d|}\varepsilon\tilde{t})], \tag{11}$$

where we additionally used the result from Eq. (9). Finally, using Taylor's series about $\tilde{t} = 0$ for $\cos[\theta_0\cos(\sqrt{|u_d|}\varepsilon\tilde{t})]$ and integrating Eq. (11) with respect to time gives

$$\begin{aligned}\tilde{x}_1 - x_{10} &= (1 + 2|u_d|\cos(\theta_0) - 3|u_d|)\tilde{t}\\ &\quad + \frac{3}{4}|u_d|\theta_0^2\tilde{t} + \frac{3\sqrt{|u_d|}\theta_0^2}{8\varepsilon}\sin(2\sqrt{|u_d|}\varepsilon\tilde{t}),\end{aligned} \tag{12}$$

where $\tilde{x}_1(0) = x_{10}$. The last step is to notice that if trapping occurs, the $\tilde{x}_1$ coordinate should be bounded, which is achieved if the ratio u_d is such that

$$u_d^* = -\frac{1}{3 - 2\cos(\theta_0) - \frac{3}{4}\theta_0^2}. \tag{13}$$

This equation is precisely the condition to observe trapping for a given small initial angle θ_0. With this result and Eq. (12), one gets that the extrema for the coordinate $\tilde{x}_1$ are $-3\sqrt{|u_d|}\theta_0^2/8\varepsilon \leqslant \tilde{x}_1 \leqslant 3\sqrt{|u_d|}\theta_0^2/8\varepsilon$, at times $\tilde{t}_1 = 3\pi/4\sqrt{|u_d|}\varepsilon$ and $\tilde{t}_2 = \pi/4\sqrt{|u_d|}\varepsilon$, respectively. Equation (13) is plotted in Fig. 2 and compared with numerical values for u_d where trapping occurs (red circles). Note that the angle is measured in radians; thus from the figure, our approximation remains valid for around $\theta_0 < 34^\circ$. Figure 3 shows that for a small variation $\delta > 0$ from u_d^*, the swimmer will perform swinging and tumbling trajectories, as found in previous works [31]. Furthermore, by applying the change of variables $X = 8\varepsilon\tilde{x}_1/3\theta_0^2\sqrt{|u_d|}$, $Y = -\varepsilon\tilde{x}_2/\theta_0\sqrt{|u_d|}$, and $s = \sqrt{|u_d|}\varepsilon\tilde{t}$ and substituting Eq. (9) into the system (6)–(8), one gets that the parametric equations for the closed orbit are $X(s) = \sin(2s)$ and $Y(s) = \sin(s)$; thus one may also represent the closed curve as

$$Y^4 - Y^2 + \tfrac{1}{4}X^2 = 0. \tag{14}$$

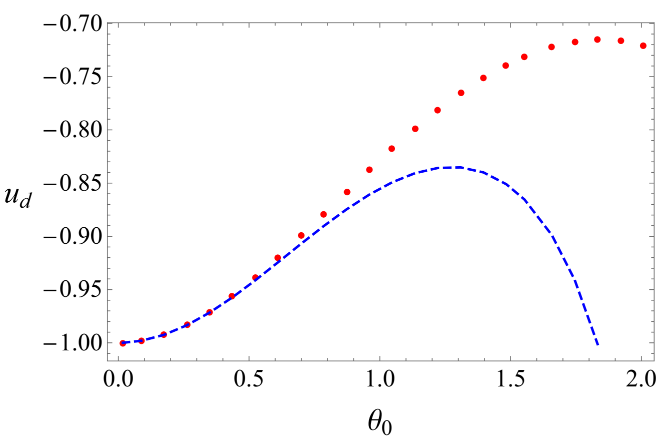

FIG. 2. Theoretical condition for u_d [Eq. (13)] in order to observe trapping (blue dashed line) and valid for small initial angles θ_0. The numerical values for u_d where trapping occurs are shown as red circles.

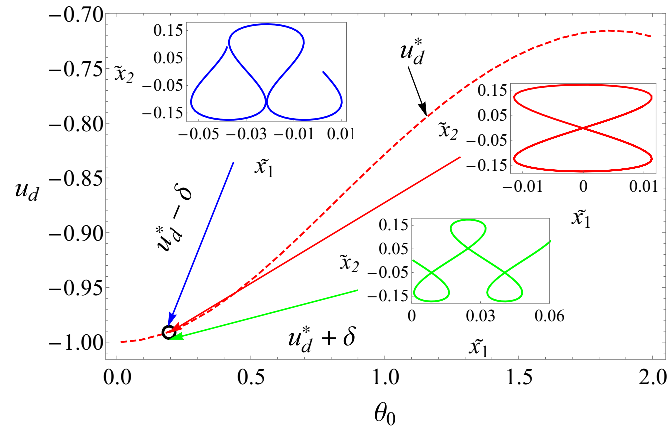

FIG. 3. A self-driven particle in a Poiseuille flow will develop closed orbits for $u_d = u_d^*$ and swinging and tumbling trajectories for $u_d = u_d^* \pm \delta$ with $\delta > 0$ as shown in the insets.

IV. MEAN-SQUARE DISPLACEMENT IN TWO DIMENSIONS

What is the effect of an external Poiseuille flow on the diffusive behavior of noninteracting active Brownian particles? This is a question that has been partially addressed by Foister and van de Ven [25]. They performed a theoretical work exploring the consequences of a Poiseuille flow on the diffusion of passive Brownian particles. They obtained that the MSD along the flow direction (from a frame moving with a velocity equal to v_m with respect to the laboratory frame) behaves as $\sim t^4$. We will also concentrate on the MSD, but of noninteracting active Brownian particles.

Due to the coupling between the stochastic rotational dynamics [Eq. (5)] and the space coordinate x_2, an explicit analytic probability distribution function (PDF) for the angular coordinate seems difficult to obtain. For this reason, we solve the system (3)–(5) numerically. Let us explore the effect of a Poiseuille flow and confinement (neglecting hydrodynamic interactions between the particle and walls) on the diffusion of the swimmer. For this analysis, the translational Péclet number, defined as $\mathrm{Pe}_U = v_m l/D_B$ (D_B is the translational diffusion coefficient $D_B = k_B T/R_U$). was fixed to $\mathrm{Pe}_U = 47\,600$ (similar to some reported experimental values [35]), while the rotational Péclet number $\mathrm{Pe}_\Omega = v_m/lD_\Omega$ (D_Ω is the rotational diffusion coefficient $D_\Omega = k_B T/R_\Omega$) was fixed to $\mathrm{Pe}_\Omega = 6.1$. Other simulations for different Péclet numbers are reported in Appendix B. Finally, the dimensionless velocity was selected

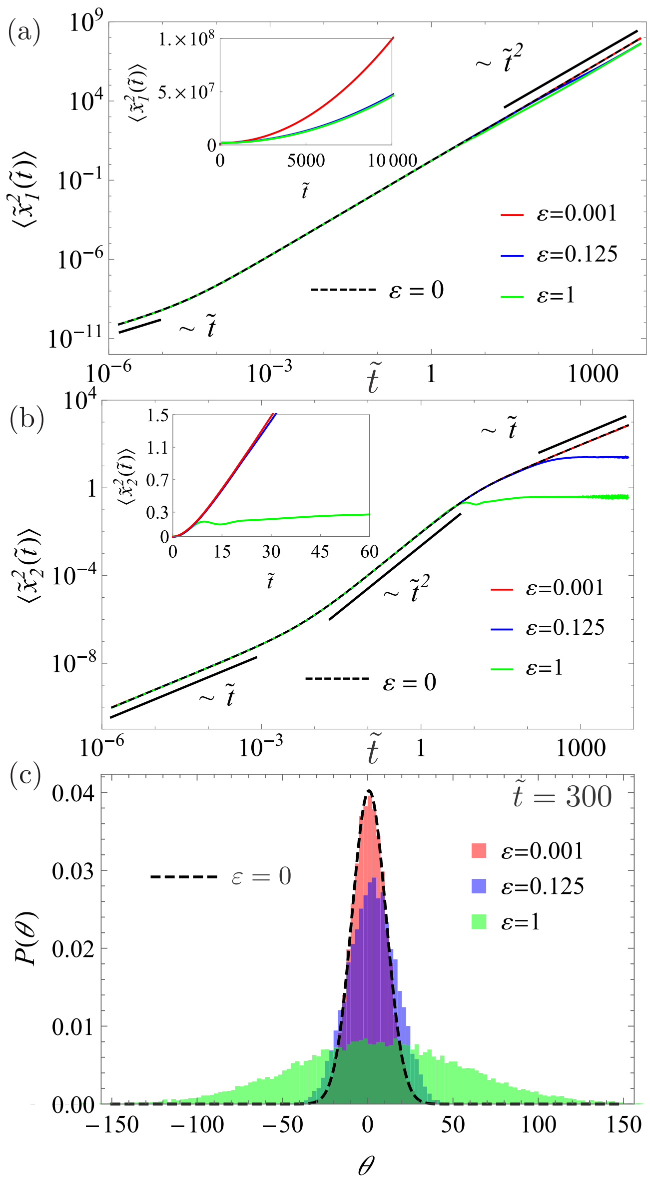

FIG. 4. Effect of a Poiseuille flow and confinement on the MSD of a swimmer moving in two dimensions and for the radii of three different channels, namely, $\varepsilon = \{0,0.125,1\}$. (a) The MSD component along the axial direction x_1. (b) The MSD component along the transversal direction x_2. In (a) and (b) the black dashed lines are theoretical results corresponding to Eqs. (A1) and (A2). (c) The PDF for the orientational coordinate showing the effect of a Poiseuille flow and confinement on its standard deviation. Clearly, the standard deviation of the angular PDF grows as $\varepsilon \to 1$.

to be $u_d = 0.1$, whereas the initial position and orientation were $\tilde{x}_1(0) = \tilde{x}_2(0) = 0$ and $\theta_0 = \pi/4$, respectively. For all the reported averages in this work, 10 000 realizations were used. The results are shown in Figs. 4(a) and 4(b), where the MSD for the $\tilde{x}_1$ and $\tilde{x}_2$ coordinates as a function of time and for the radii of three different channels (fixed $\tilde{l}$ or, equivalently, fixed v_m), namely, $\varepsilon = \{0,0.125,1\}$, is plotted. The case $\varepsilon = 0$ ($R \to \infty$), which corresponds to an unbounded domain, where the parabolic profile becomes a plane one, can be analytically solved. Taking the limit $\varepsilon \to 0$ to Eqs. (3)–(5) yields

$$\dot{\tilde{x}}_1(\tilde{t}) = 1 + u_d \cos\theta(\tilde{t}) + \tilde{f}_1(\tilde{t}), \tag{15}$$

$$\dot{\tilde{x}}_2(\tilde{t}) = u_d \sin\theta(\tilde{t}) + \tilde{f}_2(\tilde{t}), \tag{16}$$

$$\dot{\theta}(\tilde{t}) = \tilde{g}(\tilde{t}). \tag{17}$$

Since the angular coordinate is decoupled from the translational coordinate, it obeys a simple Smoluchowski equation whose PDF is

$$\begin{aligned} P(\theta,\tilde{t}|\theta_1,\tilde{t}_1) &= \frac{e^{-\mathrm{Pe}_\Omega(\theta-\theta_1)^2/4\tau}}{\sqrt{4\pi\tau/\mathrm{Pe}_\Omega}}, \\ P(\theta_1,\tilde{t}_1) &= \frac{e^{-\mathrm{Pe}_\Omega(\theta_1-\theta_0)^2/4\tilde{t}_1}}{\sqrt{4\pi\tilde{t}_1/\mathrm{Pe}_\Omega}}, \end{aligned} \tag{18}$$

where $\tau = \tilde{t} - \tilde{t}_1$, $P(\theta,\tilde{t}|\theta_1,\tilde{t}_1)$ is the conditional PDF, θ_1 is the angular coordinate at time $\tilde{t}_1 < \tilde{t}$, and $P(\theta_1,\tilde{t}_1)$ is the unconditional PDF with an initial condition $\theta_0(0) = \theta_0$. With Eq. (18), the swimmer's orientation correlations can be evaluated. They are defined as [45]

$$\langle e_k(\tilde{t})e_l(\tilde{t}_1)\rangle = \int d\theta \int d\theta_1 e_k(\tilde{t})e_l(\tilde{t}_1)G(\theta,\tilde{t};\theta_1,\tilde{t}_1), \tag{19}$$

where $G(\theta,\tilde{t};\theta_1,\tilde{t}_1) = P(\theta,\tilde{t}|\theta_1,\tilde{t}_1)P(\theta_1,\tilde{t}_1)$ is the joint probability distribution. By directly solving Eq. (19), the orientation correlations are finally obtained, namely,

$$\langle e_1(\tilde{t})e_1(\tilde{t}_1)\rangle = \frac{e^{-\tau/\mathrm{Pe}_\Omega}}{2}[1 + \cos(2\theta_0)e^{-4\tilde{t}_1/\mathrm{Pe}_\Omega}], \tag{20}$$

$$\langle e_2(\tilde{t})e_2(\tilde{t}_1)\rangle = \frac{e^{-\tau/\mathrm{Pe}_\Omega}}{2}[1 - \cos(2\theta_0)e^{-4\tilde{t}_1/\mathrm{Pe}_\Omega}], \tag{21}$$

$$\langle e_1(\tilde{t})e_2(\tilde{t}_1)\rangle = \frac{e^{-\tau/\mathrm{Pe}_\Omega}}{2}[\sin(2\theta_0)e^{-4\tilde{t}_1/\mathrm{Pe}_\Omega}]. \tag{22}$$

We then use Eqs. (15)–(17) together with the latter correlations to find the components of the MSD tensor. The full expressions of these components are given in Appendix A, whereas their long-time expressions are

$$\langle \tilde{x}_1^2(\tilde{t})\rangle = \tilde{t}^2 + \left(u_d^2\mathrm{Pe}_\Omega + \frac{2}{\mathrm{Pe}_U}\right)\tilde{t} + 2u_d\mathrm{Pe}_\Omega\cos(\theta_0)\tilde{t}, \tag{23}$$

$$\langle \tilde{x}_2^2(\tilde{t})\rangle = \left(\frac{2}{\mathrm{Pe}_U} + u_d^2\mathrm{Pe}_\Omega\right)\tilde{t}, \tag{24}$$

$$\langle \tilde{x}_1(t)\tilde{x}_2(t)\rangle = u_d\mathrm{Pe}_\Omega\sin(\theta_0)\tilde{t}. \tag{25}$$

Note that the case $\varepsilon = 0$ contains a quadratic scaling with respect to time [see Eq. (23)]. Equations (A1) and (A2) are then plotted as black dashed lines in Figs. 4(a) and 4(b) and represent an upper bound limit for the MSD components obtained numerically. Numerical results for $\varepsilon \neq 0$ (meaning that the magnitude of v_m, hence the value of l, was kept constant while varying R) are also shown in Fig. 4(a). The inset of this figure shows that the space covered by the swimmer along the axial direction increases as the channel's width increases. This is so since for small ε the particle will be dragged along the flow direction by an almost uniform flow; however, when ε increases there will be regions (near the walls) where the particle is barely dragged by the external flow. For long times, Fig. 4(a) shows that the swimmer's displacement always becomes quadratic. Finally, Fig. 4(a) also indicates that for very short times ($\tilde{t} \leqslant 10^{-5}$) the MSD behaves linearly in time; in fact, it can be shown that for this regime the MSD along the flow direction is (see Appendix A)

$$\langle \tilde{x}_1^2(\tilde{t}) \rangle = \frac{2\tilde{t}}{\mathrm{Pe}_U} + u_d \cos^2(\theta_0)\tilde{t}^2 + O(\tilde{t}^3). \tag{26}$$

Figure 4(b) shows the confinement effect along the transversal direction. We see that its MSD starts linearly in time, then it goes to a quadratic behavior, and finally for unconfined particles it reaches for long times a linear dependence again. For confined particles its MSD reaches a constant value. Confinement and the presence of a Poiseuille flow also influence the angular probability distribution function. We see in Fig. 4(c) that the standard deviation of the angular PDF grows as $\varepsilon \to 1$. In particular, we show this effect for $\tilde{t} = 300$. A proof of kurtosis and skewness indicates that this PDF for short times is not Gaussian, whereas for long times it acquires a Gaussian behavior. We also performed an analysis from a moving frame (X_1, X_2) displaced with a velocity v_m, that is, $X_1 = x_1 - v_m t$ and $X_2 = x_2$. Note that this analysis was made for small enough times in such a way that the particle does not reach the walls. We plot in Fig. 5 the MSD along the flow direction with respect to this new frame. Clearly, a quartic dependence of the MSD is also present in self-propelled Brownian particles. Note that this scaling cannot be seen in the laboratory frame where the quadratic behavior screens the quartic one. The black dashed line corresponds to the result given by Foister and van de Ven [25] for a passive Brownian particle ($u_d = 0$), namely, $\langle \tilde{X}_1^2 \rangle = 2\tilde{t}/\mathrm{Pe}_T + 7\varepsilon^2\tilde{t}^4/3\,\mathrm{Pe}_T^2$. We also see that as activity increases, the quartic behavior will disappear.

We now turn to the effect of self-propulsion and the presence of a Poiseuille flow on the swimmer's diffusion, what happens to the net displacement of a swimmer that increases its propulsion while immersed in the same Poiseuille flow. For this analysis we kept $\varepsilon = 1$, $\mathrm{Pe}_U = 47\,600$, and $\mathrm{Pe}_\Omega = 6.1$, which physically means that both the diameter of the channel (in two dimensions) or tube (in three dimensions) and the magnitude of v_m were kept constant. We varied the dimensionless velocity u_d, as $u_d = \{0, 0.01, 0.1, 0.3\}$, meaning that the particle swims faster as u_d increases. The measure of its average net displacement in time was calculated with the particle's MSD along the axial and transversal directions. For the MSD along the flow direction, Fig. 6(a) shows that the swimmer reaches longer distances as u_d decreases, in other words, a death (passive) Brownian particle will spread better. This is because an active particle may perform upstream swimming or may even become trapped as shown in Sec. III, thus retarding the displacement along the flow direction. Thermal fluctuations will eventually break the closed loops and the particle will continue moving towards the imposed direction by the flow. The inset of Fig. 6(a) shows that its MSD starts linearly in time [characterized by Eq. (26)] but that it reaches a quadratic dependence as $\tilde{t} \to \infty$. Figure 6(b) shows

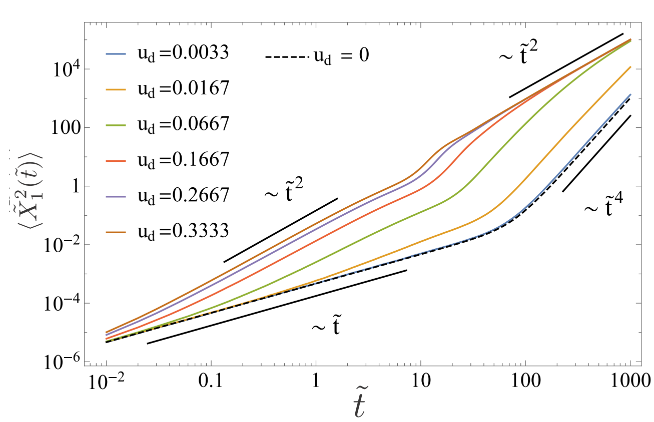

FIG. 5. The MSD along the flow direction with respect to a moving frame (X_1, X_2) displaced with a velocity v_m, that is, $X_1 = x_1 - v_m t$ and $X_2 = x_2$. In this frame the quartic time dependence can be appreciated.

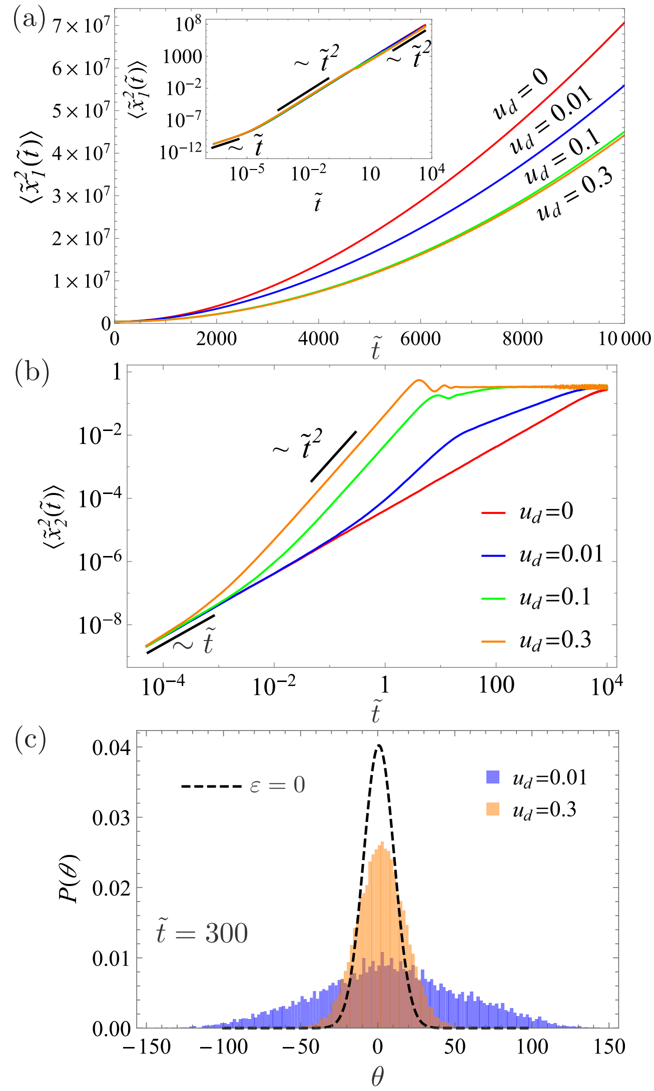

FIG. 6. Effect of a Poiseuille flow and self-propulsion on the MSD of a swimmer moving in two dimensions and confined in a channel. (a) The MSD component along the axial direction. (b) The MSD component along the transversal direction. (c) The PDF for the orientational coordinate showing the effect of self-propulsion on its standard deviation. For longer times this PDF becomes Gaussian.

that as self-propulsion increases, the transversal coordinate reaches its steady state faster, that is, self-propulsion causes the particles to reach the walls in a shorter time compared to passive ones. Self-propulsion also affects the angular PDF since for this case ($\varepsilon = 1$) rotation and translation are fully coupled. Figure 6(c) shows the angular probability distribution functions for the cases $u_d = \{0.01,0.3\}$ and for $\tilde{t} = 300$. This figure indicates that as u_d decreases the standard deviation of the angular PDF increases. It was also observed from a kurtosis and skewness test that only for long times, the orientational PDF becomes Gaussian. For comparison purposes, we show in the same figure (black dashed line) the PDF for the case when there is no coupling between the angular and translational dynamics.

V. MEAN-SQUARE DISPLACEMENT IN THREE DIMENSIONS

We generalize our study by simulating a Brownian swimmer moving in three dimensions and inside a cylinder (with specular walls that do not influence the swimmer's rotation) of radius R. This swimmer has a fully rotational freedom, that is, in a spherical coordinate system, it can rotate along the azimuthal φ and polar θ directions. For this 3D situation we define $\mathbf{x}(t) = [x_1(t), x_2(t), x_3(t)]$ and $\mathbf{e}(t) = [e_1(t), e_2(t), e_3(t)]$, with $e_1(t) = \sin\theta(t)\cos\varphi(t)$, $e_2(t) = \sin\theta(t)\sin\varphi(t)$, and $e_3(t) = \cos\theta(t)$, and we assume that the particle is subject to a Poiseuille flow of the form $\mathbf{u}_\infty = v_m[1 - x_1^2/R^2 - x_2^2/R^2]\mathbf{k}$. By nondimensionalizing Eqs. (1) and (2) in the same way as in the 2D case, the dynamics of a self-driven particle in three dimensions is dictated by

$$\dot{\tilde{x}}_1(\tilde{t}) = u_d e_1(\tilde{t}) + \tilde{f}_1(\tilde{t}), \tag{27}$$

$$\dot{\tilde{x}}_2(\tilde{t}) = u_d e_2(\tilde{t}) + \tilde{f}_2(\tilde{t}), \tag{28}$$

$$\dot{\tilde{x}}_3(\tilde{t}) = \left[1 - \varepsilon^2\tilde{x}_1^2(\tilde{t}) - \varepsilon^2\tilde{x}_2^2(\tilde{t})\right] + u_d e_3(\tilde{t}) + \tilde{f}_3(\tilde{t}), \tag{29}$$

$$\dot{\mathbf{e}}(\tilde{t}) = \tilde{\boldsymbol{\Omega}}(\tilde{t}) \times e(\tilde{t}), \tag{30}$$

where in this case the swimmer's angular velocity is given by

$$\tilde{\boldsymbol{\Omega}}(\tilde{t}) = \varepsilon^2[\tilde{x}_1(\tilde{t})\mathbf{j} - \tilde{x}_2(\tilde{t})\mathbf{i}] + \tilde{\mathbf{g}}(\tilde{t}). \tag{31}$$

Note that Eqs. (27)–(30) represent a 6×6 coupled system. We solve the latter system numerically. Let us start with the effect of a Poiseuille flow and confinement (neglecting hydrodynamic interactions between the swimmer and walls) on the swimmer's diffusion. For the simulations we consider $\mathrm{Pe}_U = 47\,600$, $\mathrm{Pe}_\Omega = 6.1$, and $u_d = 0.1$, whereas the initial position and orientations are $\tilde{x}_1(0) = \tilde{x}_2(0) = \tilde{x}_3(0) = 0$, $\theta_0 = \pi/4$, and $\varphi_0 = 0$. The results are shown in Fig. 7, where the MSD (solid lines) for the x_2 (transversal axis) and x_3 (longitudinal axis) coordinates is plotted as a function of time. Three different cylinder diameters were chosen, namely, $\varepsilon = \{0.001,0.125,1\}$. The value $\varepsilon = 0.001$ corresponds to a nearly unbounded domain where the Poiseuille flow is almost a uniform flow. In the same figure, we superpose (dashed lines) our previous 2D results. We observe that the behavior of the swimmer in a 3D situation is practically the same as in two dimensions. It can also be seen that in a 2D environment, a swimmer reaches longer distances, since in three dimensions the particle possesses two more degrees of freedom. The inset of Fig. 7(a) shows that for longer times the MSD along the flow direction scales as $\sim\tilde{t}^2$. This MSD also presents a quartic scaling (before the particle reaches the walls) that can only be seen in the same moving frame as in the 2D case. Finally, Fig. 7(b) shows the confinement effect along the transversal direction. In that figure, our previous 2D results are also superposed (dashed lines). Once again and for a given time, the particle reaches longer distances in two dimensions than in three dimensions. For both cases, the confinement effect on the MSD along the transversal direction is the same.

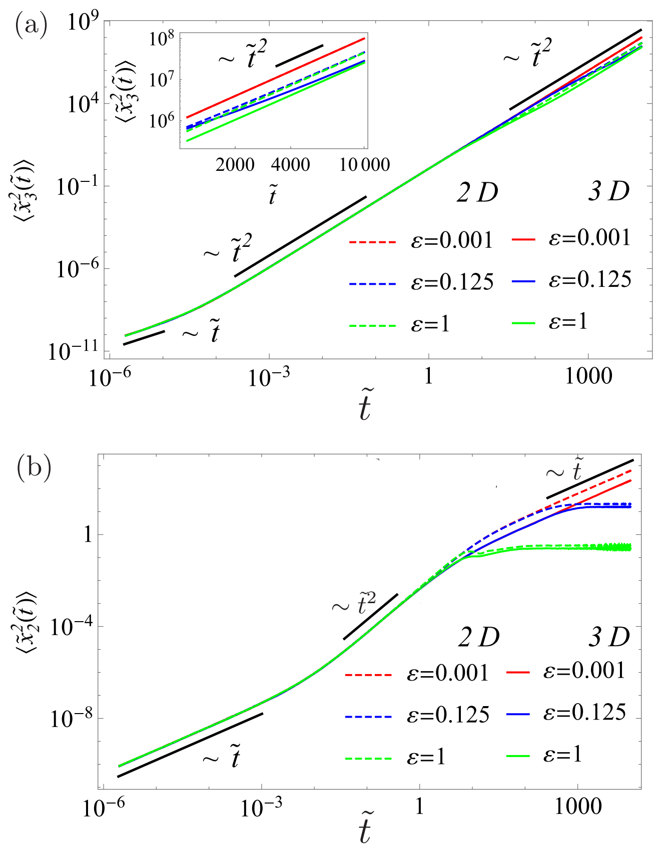

FIG. 7. Effect of a Poiseuille flow and confinement on the MSD of a swimmer moving in three dimensions and for the radii of three different channels, namely, $\varepsilon = \{0,0.125,1\}$. (a) The MSD component along the axial direction x_3. (b) The MSD component along the transversal direction x_2. The MSD for a swimmer displaced in two dimensions is also plotted for comparison purposes.

The effect of self-propulsion and the presence of a Poiseuille flow on the swimmer's diffusion in three dimensions is also studied. For this analysis we kept $\varepsilon = 1$, $\mathrm{Pe}_U = 47\,600$, and $\mathrm{Pe}_\Omega = 6.1$ and varied the dimensionless velocity as $u_d = \{0,0.01,0.1,0.3\}$; in other words, we kept the same cylinder and the same flow rate of the Poiseuille flow, but we varied the swimmer's velocity. Figure 8(a) shows the MSD along the flow direction. In accord with the 2D model (superposed in the same figure as dashed lines), one can see that the swimmer reaches longer distances as u_d decreases and that as self-propulsion increases the transversal coordinate

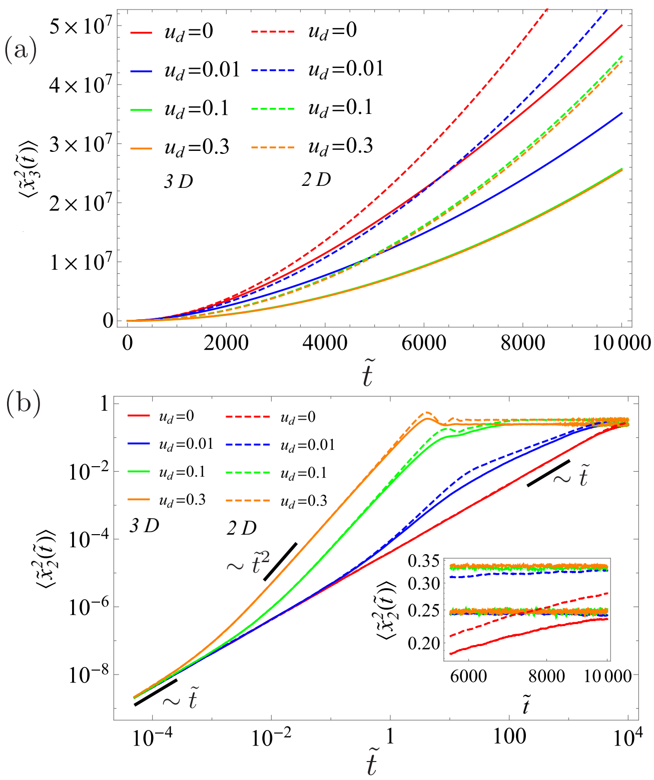

FIG. 8. Effect of a Poiseuille flow and self-propulsion on the MSD of a swimmer moving in three dimensions and confined in a cylinder. (a) The MSD component along the axial direction. (b) The MSD component along the transversal direction. The MSD for a swimmer displaced in two dimensions is also plotted for comparison purposes.

reaches its steady state faster [see Fig. 8(b)]. With the latter comparison, one corroborates that for the present system, a two-dimensional model gives qualitative results very similar to those for a fully three-dimensional one. Finally, we show that trapping of a swimmer moving in three dimensions and subject to a Poiseuille flow is also possible. The main question here is whether we can find a trapping condition for this scenario similar to Eq. (13). Our imposed flow is of the form $\mathbf{u}_\infty = v_m[1 - x_1^2/R^2 - x_2^2/R^2]\mathbf{k}$, hence it has azimuthal symmetry and thus along each plane $\varphi =$ const, the condition given by Eq. (13) should also hold in three dimensions. We thus follow that condition and impose it in our 3D numerical simulations. We choose $\theta_0 = 15^\circ$, hence we get from Eq. (13) that $u_d^* = -0.983\,532$. We also selected different azimuthal angles, namely, $\varphi = \{0^\circ, 45^\circ, 90^\circ, 135^\circ\}$. Thus, by solving Eqs. (27)–(30) in the absence of noise, under the latter conditions, we obtained the closed orbits shown in Fig. 9(a). After that, very small thermal fluctuations were systematically added and their effect on the closed orbits can be appreciated in Figs. 9(b)–9(d). The translational and rotational Péclet numbers Pe_U and Pe_Ω, respectively, used in Figs. 9(b)–9(d) were both of order $\sim 10^5$, $\sim 10^4$, and $\sim 10^3$, respectively. One can see that as the thermal noise increases, the particle no longer develops closed paths. From several simulations we observed that for longer times the swimmers will eventually leave its trapping region.

VI. HYDRODYNAMIC INTERACTIONS WITH WALLS

To take into account HEs between walls and swimmer and see their possible consequences on the particle's diffusion, we concentrate on a two-dimensional scenario (see Fig. 1) and model our active particle following the force dipole approximation [46]. This far-field theory provides the induced translational and angular velocities on the swimmer due to the presence of walls. The anisotropy of the translational diffusion coefficient due to the walls was also considered, but the rotational diffusion coefficient was kept constant in this simple model. In this sense, the translational diffusion coefficients parallel and perpendicular to the walls read [47]

$$D_\parallel = D_B\left[1 - \frac{9}{16}\left(\frac{a}{x_2 + R} + \frac{a}{x_2 - R}\right)\right],$$
$$D_\perp = D_B\left[1 + \frac{9}{8}\left(\frac{a}{x_2 + R} + \frac{a}{x_2 - R}\right)\right].$$

Within this approach, the dynamics of the Brownian swimmer in dimensionless form is

$$\dot{\tilde{x}}_1 = 1 - \varepsilon^2\tilde{x}_2^2 + u_d\cos\theta + \sqrt{\frac{2}{\mathrm{Pe}_\parallel}}W_{\tilde{x}_1} - \frac{3\tilde{p}}{64\pi}\sin\theta\cos\theta\left[\frac{1}{(1+\varepsilon\tilde{x}_2)^2} - \frac{1}{(1-\varepsilon\tilde{x}_2)^2}\right], \quad (32)$$

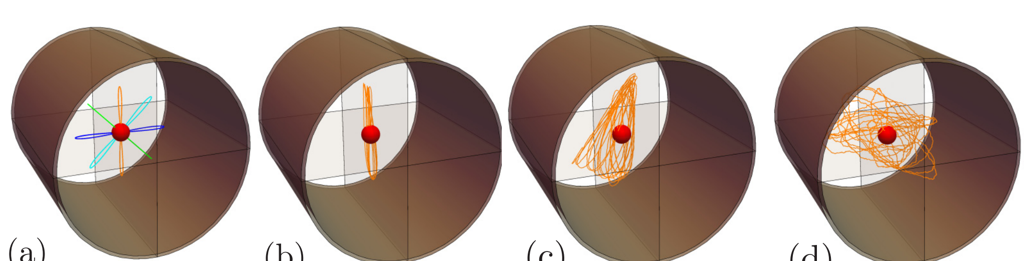

FIG. 9. Three-dimensional closed orbits and effect of thermal fluctuations on the trapping phenomenon. (a) Three possible orbits of a swimmer for an initial angle $\theta_0 = 15^\circ$ and for several azimuthal angles, namely, $\varphi = \{0^\circ, 45^\circ, 90^\circ, 135^\circ\}$. Thermal fluctuations are added that correspond to translational and rotational Péclet numbers (b) $\{\mathrm{Pe}_U, \mathrm{Pe}_\Omega\} \sim 10^5$, (c) $\{\mathrm{Pe}_U, \mathrm{Pe}_\Omega\} \sim 10^4$, and (d) $\{\mathrm{Pe}_U, \mathrm{Pe}_\Omega\} \sim 10^3$.

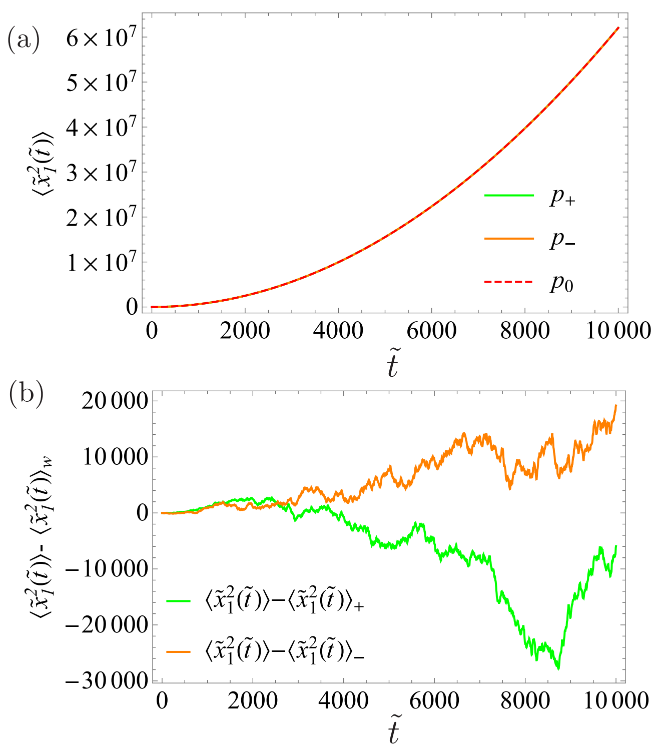

FIG. 10. (a) Comparison among the MSD of pullers p_+ and pushers p_-, both subject to hydrodynamic wall effects, and a swimmer with only specular boundary conditions p_0. (b) Difference between the MSD along the flow direction in the absence of HEs $\langle\tilde{x}_1^2(\tilde{t})\rangle$ and the MSD in the presence of HEs for pushers $\langle\tilde{x}_1^2(\tilde{t})\rangle_+$ and pullers $\langle\tilde{x}_1^2(\tilde{t})\rangle_-$.

$$\dot{\tilde{x}}_2 = u_d \sin\theta + \sqrt{\frac{2}{\mathrm{Pe}_\perp}} W_{\tilde{x}_2} - \frac{3\tilde{p}}{64\pi}(3\sin^2\theta - 1)\left[\frac{1}{(1+\varepsilon\tilde{x}_2)^2} - \frac{1}{(1-\varepsilon\tilde{x}_2)^2}\right], \tag{33}$$

$$\dot{\theta} = \varepsilon^2\tilde{x}_2 + \sqrt{\frac{2}{\mathrm{Pe}_R}} W_\theta - \frac{3\tilde{p}}{64\pi}\sin\theta\cos\theta\left[\frac{1}{(1-\varepsilon\tilde{x}_2)^3} + \frac{1}{(1+\varepsilon\tilde{x}_2)^3}\right], \tag{34}$$

where we define $\tilde{p} = p/v_m R^2\eta$, $\mathrm{Pe}_\parallel = v_m l/D_\parallel$, and $\mathrm{Pe}_\perp = v_m l/D_\perp$. Here $W_{\tilde{x}_1}$, $W_{\tilde{x}_2}$, and W_θ are independent white noise processes. In our simulations we chose the dipole strength p, equal to $p = 0.8$ pN μm for pushers and $p = -0.8$ pN μm for pullers [46]. We allowed the swimmer to approach the walls no more than $L/l = 0.1$, in accord with experimental studies [46]. Figures 10(a) and 10(b) show results for the case $\varepsilon = 0.1$, $\mathrm{Pe}_U = 119$, $u_d = 1$, $\theta_0 = \pi/4$, and $\mathrm{Pe}_\Omega = 6.1$ for 10 000 realizations and for particles initially at the origin. The symbols p_+, p_-, and p_0 indicate, respectively, that in the simulation a pusher, puller, and swimmer without HEs were considered. Figure 10(a) shows that HEs for both pushers and pullers do not seem to influence the behavior of the MSD. We additionally subtracted the MSD along the flow direction in the absence of HEs $\langle\tilde{x}_1^2(\tilde{t})\rangle$, with the MSD in the presence of HEs for pushers $\langle\tilde{x}_1^2(\tilde{t})\rangle_+$ and pullers $\langle\tilde{x}_1^2(\tilde{t})\rangle_-$. This result is shown in Fig. 10(b). One can see that such a difference oscillates around zero, hence it seems that within this model HEs do not play an important role. Probably, HE interactions could affect the swimmer's diffusion only if the radius of the channel is a few times the size of the swimmer [31].

VII. CONCLUSION

In summary, we have studied the effect of a Poiseuille flow on both a deterministic and a Brownian swimmer. It was found (theoretically and numerically) that a deterministic swimmer can perform closed orbits due to hydrodynamic forces and torques; in other words, a microsystem where a swimming particle is subject to a Poiseuille flow, under certain values for the ratio of swimming velocity and velocity of the Poiseuille flow at the center of the channel or tube, can be used as a trap. This observation could be validated by the experimental community. It was found that the combination of a Poiseuille flow and the presence of walls leads to a long-time quadratic time behavior of the MSD along the flow direction, but that this system also has a quartic time dependence before the swimmer reaches the walls. We also concluded that an active Brownian particle in a channel or tube, subject to a Poiseuille flow, travels shorter distances compared to passive Brownian particles since an active particle may perform upstream swimming or even may become trapped for a while, thus retarding the displacement along the flow direction. It was observed that a two-dimensional model of the problem gave qualitative results very similar to a more sophisticated three-dimensional study. Finally, the inclusion of hydrodynamic effects between walls and swimmer by means of a force dipole model suggested that walls do not seem to affect the particle's diffusion, at least for situations when the channel's radius is larger than a few times the size of the swimmer.

ACKNOWLEDGMENT

M.S. thanks Consejo Nacional de Ciencia y Tecnologia for support through Grant No. CB 2014/237848.

APPENDIX A: THE MSD FOR $\varepsilon = 0$ IN TWO DIMENSIONS

In this appendix we provide the whole components of the MSD tensor for the case $\varepsilon = 0$. These components are obtained by using Eqs. (15)–(17) together with the correlations (20)–(22). The MSD component along the flow direction is

$$\begin{aligned}\langle[\tilde{x}_1(\tilde{t}) - \tilde{x}_{10}]^2\rangle &= \tilde{t}^2 + \left(u_d^2\mathrm{Pe}_\Omega + \frac{2}{\mathrm{Pe}_U}\right)\tilde{t} \\ &\quad + 2u_d\mathrm{Pe}_\Omega\cos(\theta_0)(1 - e^{-\tilde{t}/\mathrm{Pe}_\Omega})\tilde{t} - u_d^2\mathrm{Pe}_\Omega^2 \\ &\quad + u_d^2\mathrm{Pe}_\Omega^2\cos(2\theta_0)\left(\frac{1}{4} + \frac{e^{-4\tilde{t}/\mathrm{Pe}_\Omega}}{12} - \frac{e^{-\tilde{t}/\mathrm{Pe}_\Omega}}{3}\right) \\ &\quad + u_d^2\mathrm{Pe}_\Omega^2 e^{-\tilde{t}/\mathrm{Pe}_\Omega}\end{aligned} \tag{A1}$$

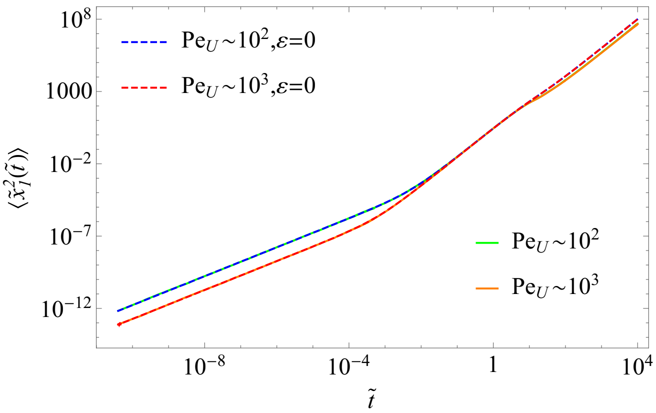

FIG. 11. The MSD along the flow direction for two different Péclet numbers, namely, $\mathrm{Pe}_U \sim 100$ and $\mathrm{Pe}_U \sim 1000$. Solid lines correspond to numerical simulations, while dashed lines correspond to the theoretical equation (A1).

while for the transversal direction we get

$$\begin{aligned}\langle[\tilde{x}_2(\tilde{t}) - \tilde{x}_{20}]^2\rangle &= \left(u_d^2\mathrm{Pe}_\Omega + \frac{2}{\mathrm{Pe}_U}\right)\tilde{t} - u_d^2\mathrm{Pe}_\Omega^2 - u_d^2\mathrm{Pe}_\Omega^2\cos(2\theta_0)\\ &\times\left(\frac{1}{4} + \frac{e^{-4\tilde{t}/\mathrm{Pe}_\Omega}}{12} - \frac{e^{-\tilde{t}/\mathrm{Pe}_\Omega}}{3}\right) + u_d^2\mathrm{Pe}_\Omega^2 e^{-\tilde{t}/\mathrm{Pe}_\Omega}. \qquad \text{(A2)}\end{aligned}$$

In addition, the cross-correlation component is

$$\begin{aligned}&\langle[\tilde{x}_1(\tilde{t}) - \tilde{x}_{10}][\tilde{x}_2(\tilde{t}) - \tilde{x}_{20}]\rangle\\ &= u_d\mathrm{Pe}_\Omega\sin(\theta_0)(1 - e^{-\tilde{t}/\mathrm{Pe}_\Omega})\tilde{t}\\ &+ u_d^2\mathrm{Pe}_\Omega^2\cos(\theta_0)\sin(\theta_0)\left(\frac{1}{2} + \frac{e^{-4\tilde{t}/\mathrm{Pe}_\Omega}}{6} - \frac{2e^{-\tilde{t}/\mathrm{Pe}_\Omega}}{3}\right). \qquad \text{(A3)}\end{aligned}$$

APPENDIX B: SIMULATIONS FOR OTHER PÉCLET NUMBERS

In this Appendix we provide a plot (see Fig. 11) for the MSD along the flow direction with the parameters $\varepsilon = 0.1$, $u_d = 1$, and $\theta_0 = \pi/4$ for 10 000 realizations, for particles initially at the origin and for two different Péclet numbers, that is, $\mathrm{Pe}_U \sim 100$ and $\mathrm{Pe}_U \sim 1000$. One can see that its MSD will always follow a (long-time) quadratic time dependence. Their corresponding theoretical MSD expressions [Eq. (A1)] for $\varepsilon = 0$ are also plotted in red and blue dashed lines. For short times, theory coincides with the simulations, but for longer times the MSD from the simulations is smaller than the theoretical case.

[1] P. S. Lovely and F. W. Dahlquist, J. Theor. Biol. **50**, 477 (1975).
[2] T. J. Pedley and J. O. Kessler, Annu. Rev. Fluid Mech. **24**, 313 (1992).
[3] H. C. Berg, *Random Walks in Biology* (Princeton University Press, Princeton, 1993).
[4] T. Ishikawa and T. J. Pedley, J. Fluid Mech. **588**, 437 (2007).
[5] J. R. Howse, R. A. L. Jones, A. J. Ryan, T. Gough, R. Vafabakhsh, and R. Golestanian, Phys. Rev. Lett. **99**, 048102 (2007).
[6] P. Romanczuk, M. Bar, W. Ebeling, B. Lindner, and L. Schimansky-Geier, Eur. Phys. J. Spec. Top. **202**, 1 (2012).
[7] E. Lauga and T. Powers, Rep. Prog. Phys. **72**, 096601 (2009).
[8] F. Jülicher and J. Prost, Eur. Phys. J. E **29**, 27 (2009).
[9] B. Gottenbos, D. W. Grijpma, H. C. van der Mei, J. Feijen, and H. J. Busscher, J. Antimicrobial Chemother. **48**, 7 (2001).
[10] B. Gottenbos, H. C. van der Mei, F. Klatter, D. W. Grijpma, J. Feijen, P. Nieuwenhuis, and H. J. Busscher, Biomaterials **24**, 2707 (2003).
[11] K. Hori and S. Matsumoto, Biochem. Eng. J. **48**, 424 (2010).
[12] J. S. Guasto, R. Rusconi, and R. Stocker, Annu. Rev. Fluid Mech. **44**, 373 (2012).
[13] D. L. Koch and G. Subramanian, Annu. Rev. Fluid Mech. **43**, 637 (2011).
[14] M. Marchetti, J. Joanny, S. Ramaswamy, T. Liverpool, J. Prost, M. Rao, and R. A. Simha, Rev. Mod. Phys. **85**, 1143 (2013).
[15] J. J. Abbott, K. E. Peyer, M. C. Lagomarsino, L. Zhang, L. Dong, I. K. Kaliakatsos, and B. J. Nelson, Int. J. Robot. Res. **28**, 1434 (2009).
[16] G. Kosa, P. Jakab, G. Szekely, and N. Hata, Biomed. Microdevices **14**, 165 (2012).
[17] W. Gao, R. Dong, S. Thamphiwatana, J. Li, W. Gao, L. Zhang, and J. Wang, ACS Nano **8**, 12041 (2014).
[18] D. Ahmed, M. Lu, A. Nourhani, P. E. Lammert, Z. Stratton, H. S. Muddana, V. H. Crespi, and T. J. Huang, Sci. Rep. **5**, 9744 (2015).
[19] T. E. Mallouk and A. Sen, Sci. Am. **300**, 72 (2009).
[20] W. F. Paxton, S. Sundararajan, T. E. Mallouk, and A. Sen, Angew. Chem. Int. Ed. **45**, 5420 (2006).
[21] T. Mirkovic, N. S. Zacharia, G. D. Scholes, and G. A. Ozin, ACS Nano **4**, 1782 (2010).
[22] G. Li, L.-K. Tam, and J. X. Tang, Proc. Natl. Acad. Sci. U.S.A. **105**, 18355 (2008).
[23] R. Rusconi and R. Stocker, Curr. Opin. Microbiol. **25**, 1 (2015).
[24] J. Wang and W. Gao, ACS Nano **6**, 5745 (2012).
[25] R. T. Foister and T. G. M. van de Ven, J. Fluid Mech. **96**, 105 (1980).
[26] M. S. Jones, L. L. Baron, and T. J. Pedley, J. Fluid Mech. **281**, 137 (1994).
[27] R. N. Bearon and T. J. Pedley, Bull. Math. Biol. **62**, 775 (2000).
[28] B. ten Hagen, R. Wittkowski, and H. Lowen, Phys. Rev. E **84**, 031105 (2011).
[29] M. Sandoval, N. K. Marath, G. Subramanian, and E. Lauga, J. Fluid Mech. **742**, 50 (2014).
[30] M. Sandoval and A. Jimenez, J. Biol. Phys. **42**, 199 (2016).
[31] A. Zöttl and H. Stark, Phys. Rev. Lett. **108**, 218104 (2012).
[32] A. Zöttl and H. Stark, Eur. Phys. J. E **36**, 1 (2013).
[33] A. Costanzo, R. Di Leonardo, G. Ruocco, and L. Angelani, J. Phys.: Condens. Matter **24**, 065101 (2012).
[34] S. Chilukuri, C. H. Collins, and P. T. Underhill, J. Phys.: Condens. Matter **26**, 115101 (2014).

[35] R. Rusconi, J. S. Guasto, and R. Stocker, Nat. Phys. **10**, 212 (2014).
[36] K. D. Young, Microbiol. Mol. Biol. Rev. **70**, 660 (2006).
[37] R. Golestanian, T. B. Liverpool, and A. Ajdari, New J. Phys. **9**, 126 (2007).
[38] J. F. Brady, J. Fluid Mech. **667**, 216 (2010).
[39] S. Thutupalli, R. Seemann, and S. Herminghaus, New J. Phys. **13**, 073021 (2011).
[40] M. Schmitt and H. Stark, Europhys. Lett. **101**, 44008 (2013).
[41] H. C. Berg, *E. coli in Motion* (Springer, New York, 2004).
[42] M. Doi and S. Edwards, *The Theory of Polymer Dynamics* (Clarendon, Oxford, 1999).
[43] W. Coffey, Y. Kalmikov, and Y. Valdron, *The Langevin Equation: With Applications in Physics, Chemistry and Electrical Engineering* (World Scientific, Hackensack, 1996).
[44] X. Zheng, B. ten Hagen, A. Kaiser, M. Wu, H. Cui, Z. Silber-Li, and H. Löwen, Phys. Rev. E **88**, 032304 (2013).
[45] B. J. Berne and R. Pecora, *Dynamic Light Scattering: With Applications to Chemistry, Biology, and Physics* (Dover, New York, 2000).
[46] A. P. Berke, L. Turner, H. C. Berg, and E. Lauga, Phys. Rev. Lett. **101**, 038102 (2008).
[47] B. Lin, J. Yu, and S. A. Rice, Phys. Rev. E **62**, 3909 (2000).